RESEARCH PAPERS

Acta Cryst. (1997). B**53**, 851–860

Re-Refinement of Composite Modulated $Nb_2Zr_{x-2}O_{2x+1}$ ($x = 8$) Using Synchrotron Radiation Data

SIEGBERT SCHMID,[a]* JOHN G. THOMPSON,[a] RAY L. WITHERS,[a] VÁCLAV PETŘÍČEK,[b] NOBUO ISHIZAWA[c] AND SHUNJI KISHIMOTO[d]

[a]*Research School of Chemistry, Australian National University, Canberra, ACT 0200, Australia,* [b]*Institute of Physics, Academy of Sciences of the Czech Republic, Cukrovarnicka 10, 162 00 Praha 6, Czech Republic,* [c]*Research Laboratory of Engineering Materials, Tokyo Institute of Technology, Nagatsuta, Midori-ku, Yokohama 226, Japan, and* [d]*National Laboratory for High Energy Physics, Oho, Tsukuba 305, Japan. E-mail: schmid@rsc.anu.edu.au*

(*Received 14 January 1997; accepted 22 April 1997*)

Dedicated to Professor J. Strähle on the occasion of his 60th birthday

Abstract

The crystal structure of $Nb_2Zr_{x-2}O_{2x+1}$, $x = 8$, has been re-refined as a composite modulated structure using synchrotron radiation data measured at energies below the Zr *K* absorption edge. The structure comprises one-atom thick layers of two substructures stacked alternately along the **b** direction. The two component substructures are, in general, mutually incommensurable along their common *a*-axis directions and are referred to as the metal substructure (*M*), space group *Amma*, $a_M = 5.1348\,(2)$, $b_M = 4.9590\,(2)$, $c_M = 5.2908\,(3)$ Å, and the oxygen substructure (*O*), space group *Imam*, $a_O = 2.4164$, $b_O = b_M = b$, $c_O = c_M = c$, respectively. The four basis vectors used to index reciprocal space, based on the more strongly scattering metal substructure, are $\mathbf{a}_M^*$, $\mathbf{b}^*$, $\mathbf{c}^*$ and $\mathbf{q}_M$. The primary modulation wavevector $\mathbf{q}_M = \mathbf{a}_O^* - 2\mathbf{a}_M^* + \mathbf{b}^* = 1/8\,\mathbf{a}_M^* + \mathbf{b}^*$ for $x = 8$. The overall superspace-group symmetry is $Amma(\alpha 10)0s0$. Two sets of intensity data recorded at room temperature, 8 eV ($\lambda_n = 0.6892$ Å) and 1450 eV ($\lambda_f = 0.7492$ Å) below the Zr *K* absorption edge, were refined to an overall $R(\lambda_n) = 0.0377$ and $R(\lambda_f) = 0.0439$. The displacive modulation wave amplitudes obtained from these refinements agree well with those previously obtained for an $x = 12$ member. Difference Fourier maps show that metal-atom ordering is virtually negligible.

1. Introduction

Incommensurate phases can be conveniently divided into incommensurately modulated structures, incommensurate intergrowth compounds and quasicrystals (see, for example, van Smaalen, 1995). This contribution focuses on a particular intergrowth compound, $Nb_2Zr_{x-2}O_{2x+1}$, $x = 8$. Such intergrowth compounds can exist either as a homologous series of discrete line phases (as, for example, in the lanthanide halides Ln_nX_{2n+1}: Rinck, 1982; Makovicky & Hyde, 1992) or as wide range, non-stoichiometric solid solutions [as for the $(1-x)Ta_2O_5.xWO_3$ system: Roth, 1981; Schmid, Withers & Thompson, 1992; or the $Zr(N,O,F)_x$ system: Schmid & Withers, 1994]. The structures of such solid solutions have the ability to adapt continuously over an often extremely wide composition range, while maintaining the essential integrity of their structure type. Detailed crystallographic results are required across such solid solution fields in order to better understand the crystal chemical origin of this extraordinary structural flexibility.

Just such a wide range solid solution is known to exist at the ZrO_2-rich end of the ZrO_2–Nb_2O_5 system (Roth, Waring, Brower & Parker, 1972). The compositional width of this $Nb_2Zr_{x-2}O_{2x+1}$ solid solution has been reported as $7.1 \leq x \leq 10.3$ when synthesized *via* a solid-state reaction (Thompson, Withers, Sellar, Barlow & Hyde, 1990). If the synthesis is carried out *via* a flux method, however, x can be as high as 12 (Fütterer, Schmid, Thompson, Withers, Ishizawa & Kishimoto, 1995). It has previously been shown that the structures within this $Nb_2Zr_{x-2}O_{2x+1}$ solid-solution field are best described as composite modulated structures rather than as a homologous series of closely related phases (Thompson *et al.*, 1990).

The composite modulated structure at any particular x value is built from one-atom thick layers of two substructures stacked alternately along the **b** direction. The two parent substructures (a metal-atom, or *M*, substructure and an oxygen-atom, or *O*, substructure) have identical **b** and **c** axes, but are, in general, mutually incommensurable along **a** with a relative periodicity given by $\mathbf{a}_O = x/2x + 1\ \mathbf{a}_M$. Each substructure modulates the other with a primary modulation wavevector, which links the reciprocal lattices of the two parent substructures. Characterization of such a composite modulated structure requires determination of each parent substruc-

ture together with the atomic modulation functions [AMF's (Withers, Thompson & Hyde, 1991)], describing the compositional and/or displacive deviations of atoms away from their average occupancies and positions in each underlying parent substructure arising from its interaction with the other parent substructure. The primary modulation wavevector characteristic of the more strongly scattering M substructure is chosen to be $\mathbf{q}_M = [110]^*_O - [200]^*_M = (1/x)\mathbf{a}^*_M + \mathbf{b}^*_M$ (Thompson *et al.*, 1990) and is stoichiometry determined. Such an approach allows the direct structural comparison of AMF's associated with quite different compositions, *i.e.* values of x. Note that occupational as well as displacive modulation is possible in the case of the $Nb_2Zr_{x-2}O_{2x+1}$ system.

A previously reported structure for the $x = 10$ member of the closely related $Ta_2Zr_{x-2}O_{2x+1}$ solid solution field (Fig. 30 of Makovicky & Hyde, 1981) showed Ta/Zr ordering and suggests that metal ordering should also occur in the case of the $Nb_2Zr_{x-2}O_{2x+1}$ system. A recent composite modulated structure refinement (Fütterer *et al.*, 1995) of the $x = 12$ member of the $Nb_2Zr_{x-2}O_{2x+1}$ solid solution, however, found no evidence for such metal-atom ordering, despite the measurement of intensity data at an appropriately chosen synchrotron radiation wavelength in order to enhance the Zr/Nb scattering contrast. The high Zr:Nb ratio of 5:1 for $x = 12$ made any such ordering difficult to detect. One aim of the present investigation of the $x = 8$ member of the solid solution field (Zr:Nb ratio of 3:1) was to search for metal ordering at a composition where any such ordering should be more easily detected. A further aim was to investigate whether the refined AMF's (describing the structural deviation from the underlying parent substructures) are essentially the same across the whole solid solution field, *i.e.* to investigate whether all occurring structures can be regarded as being equivalent from the 'higher-dimensional' viewpoint of a composite crystal. This has previously been shown to be the case for several systems [*e.g.* $(1-x)Ta_2O_5.xWO_3$ (Schmid, Thompson, Rae, Butler, Withers, Ishizawa & Kishimoto, 1995) and $Zr(N,O,F)x$ (Schmid & Withers, 1996)].

The $x = 8$ member of the $Nb_2Zr_{x-2}O_{2x+1}$ solid solution with a primary modulation wavevector given by $\mathbf{q}_M = 1/8\ \mathbf{a}^*_M + \mathbf{b}^*_M$ has previously been refined as a conventional eight times $\mathbf{a}_M$ superstructure (Galy & Roth, 1973). As the composition-dependent component of the wavevector equals 1/8 exactly within experimental error, a question arises as to whether the phase is best described as commensurate or incommensurately modulated. Whereas theoretically a formal difference can be made between commensurate and incommensurate modulation, there is no sharp border from an empirical point of view. A continuous change of wavevector with temperature or, as in our case, composition has often been taken as one of the few definite signs of the incommensurate character of a structure (Pérez-Mato, Madariaga, Zúñiga & Garcia Arribas, 1987). A further indication has been whether or not all possible higher-order satellite reflections occur (Pérez-Mato, 1991). In the $x = 12$ case (Fütterer *et al.*, 1995) satellite reflections up to fourth order (metal subsystem) have been observed. For the present $x = 8$ member this leads to overlap between satellite reflections, *e.g.* $\mathbf{G} + 4\mathbf{q} = \mathbf{G}' - 4\mathbf{q}$, resulting in an apparent commensurateness of the structure (Pérez-Mato *et al.*, 1987). This commensurateness formally destroys the uniqueness of both the superspace-group assignment as well as the definition of the primary modulation wavevector (Withers *et al.*, 1991; Pérez-Mato *et al.*, 1987). A final aim of the present investigation therefore was to consider carefully all refinement options and examine whether the $x = 8$ structure is equally well described as a commensurate or an incommensurate intergrowth compound.

2. Experimental

2.1. *Synthesis*

Single crystals of $Nb_2Zr_{x-2}O_{2x+1}$ ($x = 8$) were grown by heating a mechanically mixed 5:1 mixture of ZrO_2 and Nb_2O_5 at 1763 K for 2 d in a sealed platinum tube. The reaction product was cooled quickly to room temperature. Clear, pale yellow prismatic single crystals of $Nb_2Zr_{x-2}O_{2x+1}$ with $x = 8$ were obtained *via* this route. Quantitative energy dispersive X-ray spectroscopic analysis using a scanning electron microscope (SEM; Jeol 6400) showed that the composition of the crystals was exactly in a ratio of 3:1 for Zr:Nb (standards used: Zr; Ta_2O_5). The crystal chosen for intensity measurements approximated a square prism of dimensions 12 x 10 x 6 μm^3 (= 7.2 x 10^2 μm^3). In principle, crystals can be grown at any value of x within the solid solution field. Limitations imposed by the data collection software, however, require x to be a relatively simple rational or integer value.

2.2. *Intensity measurement*

Preliminary tests of crystal quality – magnitude of the wavevector $\mathbf{q}_M$ and reflection profiles – were performed on a Rigaku AFC-6*R* four-circle diffractometer with rotating Cu anode. The crystals were mounted on tapered glass fibres with the diameter of the fibre ends being of approximately the same size as the crystals.

The intensity data measurement was carried out using the four-circle diffractometer at BL-14A of the Photon Factory, Tsukuba (Satow & Iitaka, 1989). Synchrotron radiation from a vertical wiggler was monochromated by a Si(111) double crystal monochromator and focused using a curved mirror. The polarization ratio, *i.e.* the fraction of the total incident beam intensity with its electrical vector vertical, is 0.95. In order to determine precisely the location of the Zr K absorption edge prior to intensity data collection, a near-edge absorption spec-

Table 1. *Important parameters*

Diffractometer	Single detector, four-circle diffractometer at vertical wiggler port BL-14A, Photon Factory					
Radiation (Å)	λ_n = 0.6892 (4)			λ_f = 0.7492 (4)		
Energy difference to Zr *K* edge (eV)	8			1450		
Monochromator	Si(111) double crystal monochromator					
$\Delta f'$, $\Delta f''$, Zr	−7.037	0.529		−2.053	0.616	
Nb	−2.414	0.588		−1.658	0.684	
O	0.010	0.006		0.012	0.007	
Scan mode	$2\theta/\omega$ scans, $\Delta\omega$ = 0.5°					
Scan speed (° min^{-1})	8			16		
Data collection limits in 2θ, *hklm*	$1 \le 2\theta \le 68°$ $-8 \le h \le 8$ $-10 \le k \le 11$ $-8 \le l \le 0$ $-4 \le m \le 4$			$1 \le 2\theta \le 70°$ $-8 \le h \le 8$ $-10 \le k \le 11$ $-8 \le l \le 0$ $-4 \le m \le 4$		
No. of measured reflections	4659; unique: 1239; unique and $I \ge 3\sigma(I)$: 575			9208; unique: 1157; unique and $I \ge 3\sigma(I)$: 623		
Standard reflections	9 reflections, measured after every 200 reflections					
Lattice parameters (Å)	41.0783 (16) = 8 × 5.1348, 4.9590 (2), 5.2908 (3) determined from 24 reflections, $33 \le 2\theta \le 48°$, at λ_n					
Modulation wavevector	$\mathbf{q}_M = 1/8\ \mathbf{a}_M^* + \mathbf{b}^*$					
Lp correction	*Xtal*3.2 (Hall, Flack & Stewart, 1992)					
Absorption correction/coefficient (mm^{-1})	No/6.41			No/8.12		
No. of reflections/unique/R_{int} (%), $I \ge 3\sigma(I)$						
All	1607	575	2.99	1725	623	3.26
m = 0	632	193	1.37	616	187	2.09
m = 1	473	159	4.27	515	159	4.21
m = 2	423	152	5.42	474	175	4.58
m = 3	57	49	13.76	100	72	10.78
m = 4	22	22	9.66	20	30	7.92

trum of ZrO_2 powder was recorded. The location of the Zr absorption edge was used to calibrate the monochromator angles with respect to the absolute incident energy. The precision of this value is limited by the width of the absorption edge, which spans several eV in our experimental data. The edge was defined as the monochromator position that corresponded to the point where absorption had risen half-way to its far-edge value. All other settings of the incident X-ray energy were defined relative to this value. Decay of the incident beam and spontaneous fluctuations were monitored with an ion chamber to enable normalization of the raw counts. There was no significant change in intensity once the data had been corrected for the variation of the incident beam resulting from decay of the synchrotron ring current.

Intensity data were recorded at two wavelengths, 1450 and 8 eV, below the Zr *K* absorption edge. The relevant parameters for the data collection are given in Table 1. To improve counting statistics on the weaker reflections, scans were repeated when $\sigma(F)/F$ was larger than 0.01, $\sigma(F)$ being calculated from counting statistics only. The maximum number of scans was 3. The data were corrected for Lorentz and polarization effects. Symmetry-equivalent reflections were averaged in the Laue group *mmm* (see Table 1).

3. Symmetry

The superspace-group symmetry at a general composition within the solid solution was previously derived (Withers *et al.*, 1991) *via* a combination of electron diffraction and a modulation wave approach based on the structure refinement of $Nb_2Zr_6O_{17}$ (Galy & Roth, 1973). Note, however, that the choice of primary modulation wavevector and indeed assignment of the superspace group is no longer formally unique if the primary modulation wavevector is commensurable with respect to the underlying substructures, as in the present $x = 8$ case (Withers *et al.*, 1991; Pérez-Mato *et al.*, 1987). The previously observed continuous compositional flexibility of the solid solution (Thompson *et al.*, 1990) nonetheless justifies treating the $x = 8$ member analogously to any other member. Relevant details as regards the consequences of superspace-group symmetry were given by Fütterer *et al.* (1995) and the following provides a summary of important details, including origin choice and settings.

(i) The $Nb_2Zr_{x-2}O_{2x+1}$ solid solution can be regarded as a (3 + 1)-dimensional composite modulated structure, consisting of two subsystems – a metal-ion, or *M*, subsystem and an oxygen-ion, or *O*, subsystem. The lattice parameters for $x = 8$ are given in Table 1.

(ii) The primary modulation wavevector of the metal subsystem is defined as $\mathbf{q}_M = [110]_O^* - [200]_M^* = \mathbf{a}_O^* - 2\mathbf{a}_M^* + \mathbf{b}^* = (1/x)\mathbf{a}_M^* + \mathbf{b}^*$ [$= (1/8)\mathbf{a}_M^* + \mathbf{b}^*$ in the present case], whereas the primary modulation wavevector of the oxygen subsystem is defined as $\mathbf{q}_O = \mathbf{a}_M^* = (8/17)\ \mathbf{a}_O^*$ (in the present case).

(iii) All reflections are indexed with respect to the more strongly scattering *M* substructure, *i.e.* the four

Table 2. *Refinement statistics for* λ_n *and* λ_f

(*a*) λ_n

Label of refinement run	N1		N2		N3		N4		N5		N6	
δ	i.c.		i.c./overlap		0.0		0.03125		i.c./overlap		0.03125	
Occupational modulation	No		No		No		No		Yes		Yes	
No. of refined parameters	27		27		27		27		29		29	
Weight	$1/\sigma(F)^2 + 0.01F^2$											
Residuals *R*, *wR* in %												
Overall	3.80	4.00	3.77	3.88	4.88	4.96	3.62	3.72	3.72	3.79	3.56	3.63
$m = 0$	2.25	2.49	2.30	2.55	2.75	2.97	2.22	2.46	2.28	2.53	2.17	2.41
$m = 1$	5.03	5.67	5.16	5.81	6.50	7.30	5.01	5.65	5.35	5.88	5.23	5.78
$m = 2$	7.07	8.11	7.05	8.10	9.63	10.6	6.47	7.49	6.89	7.86	6.34	7.31
$m = 3$	17.0	20.1	15.7	18.1	21.5	23.8	15.4	17.7	13.3	16.1	13.7	16.0
$m = 4$	29.7	37.6	16.8	19.4	37.1	41.6	19.2	21.4	10.1	13.3	13.0	15.2

(*b*) λ_f

Label of refinement run	F1		F2		F3		F4	
δ	i.c.		i.c./overlap		0.0		0.03125	
Occupational modulation	No		No		No		No	
No. of refined parameters	27		27		27		27	
Weight	$1/\sigma(F)^2$							
Residuals *R*, *wR* in %								
Overall	4.41	3.94	4.39	3.91	5.49	4.72	4.34	3.85
$m = 0$	2.59	2.83	2.57	2.82	3.01	3.10	2.58	2.82
$m = 1$	5.83	6.57	5.94	6.73	7.59	8.40	5.86	6.63
$m = 2$	8.05	9.06	8.02	8.94	10.0	10.9	6.62	8.50
$m = 3$	16.8	19.8	16.6	19.8	21.3	25.6	17.0	19.8
$m = 4$	29.7	38.0	26.5	31.4	54.4	63.3	27.8	32.5

Table 3. *Coordinates and displacive Fourier terms*

Label of Ref.	N2		N5		F2	
Zr, Nb 1/4, 0, z	0.21134 (6)		0.21129 (6)		0.21171 (7)	
$\varepsilon_x(2\mathbf{q})$, $\varepsilon_x(4\mathbf{q})$	0.02496 (8)	0.0037 (2)	0.0248 (1)	0.0021 (3)	0.02506 (9)	0.0047 (2)
$\varepsilon_y(\mathbf{q})$, $\varepsilon_y(3\mathbf{q})$	0.01801 (8)	0.0071 (2)	0.01795 (8)	0.0067 (2)	0.01792 (9)	0.0063 (2)
$\varepsilon_z(2\mathbf{q})$, $\varepsilon_z(4\mathbf{q})$	−0.0023 (1)	−0.0046 (3)	−0.0023 (1)	−0.0045 (3)	−0.0020 (1)	−0.0036 (4)
O 1/4, y, 1/2	0.2726 (3)		0.2726 (3)		0.2732 (5)	
$\varepsilon_x(2\mathbf{q})$, $\varepsilon_x(4\mathbf{q})$	−0.1733 (9)	0.036 (1)	−0.1734 (9)	0.037 (1)	−0.174 (1)	0.037 (1)
$\varepsilon_x(6\mathbf{q})$, $\varepsilon_x(8\mathbf{q})$	−0.010 (1)	0.012 (1)	−0.010 (1)	0.012 (1)	−0.011 (2)	0.011 (2)
$\varepsilon_y(2\mathbf{q})$, $\varepsilon_y(4\mathbf{q})$	−0.0838 (4)	−0.0015 (6)	−0.0838 (4)	0.0011 (6)	−0.0831 (6)	0.0014 (8)
$\varepsilon_y(6\mathbf{q})$, $\varepsilon_y(8\mathbf{q})$	0.0068 (7)	0.0091 (7)	0.0065 (7)	0.0085 (7)	0.0068 (9)	0.007 (1)
$\varepsilon_z(\mathbf{q})$, $\varepsilon_z(3\mathbf{q})$	−0.1344 (5)	0.0181 (6)	−0.1342 (5)	0.0183 (6)	−0.1356 (7)	0.0178 (8)
$\varepsilon_z(5\mathbf{q})$, $\varepsilon_z(7\mathbf{q})$	0.0146 (7)	0.0059 (8)	0.0151 (6)	0.0059 (8)	0.0137 (9)	0.005 (1)

basis vectors used to index reciprocal space are $\mathbf{a}_M^*$, $\mathbf{b}^*$, $\mathbf{c}^*$ and $\mathbf{q}_M$. The matrix W (see van Smaalen, 1991), transforming the metal-ion subsystem into the oxygen-ion subsystem, is given by

$$W = \begin{bmatrix} 2 & -1 & 0 & 1 \\ 0 & 1 & 0 & 0 \\ 0 & 0 & 1 & 0 \\ 1 & 0 & 0 & 0 \end{bmatrix},$$

$$\text{with } (\mathbf{a}^*, \mathbf{b}^*, \mathbf{c}^*, \mathbf{q})_O = (\mathbf{a}^*, \mathbf{b}^*, \mathbf{c}^*, \mathbf{q})_M W^T,$$

where W^T is the transposed matrix. Thus, $(hklm)_M = (m, k+m, l, h-2m)_O$, *i.e.* an mth-order satellite reflection of the M substructure is a $(h-2m)$th-order satellite reflection of the O substructure.

(iv) The extinction conditions characteristic of the solid solution are given by $F(hklm) = 0$ unless $k + l = 2n$, $F(hk0m) = 0$ unless $h = 2n$ and $F(hkl,-k) = 0$ unless $k = 2n$. The corresponding implied superspace-symmetry operations are $\{\mathrm{E}\ 1|0,1/2,1/2,\ 0\}$, $\{\sigma_z\ 1|\ 1/2,\ 0,\ 0,\ 0\}$ and $\{\sigma_y\ 1|\ 0,\ 0,\ 0,\ 1/2 - 2y\}$, respectively. The (3 + 1)-dimensional superspace group for the metal-ion subsystem and, by definition, for the whole crystal is *Amma* $(1/x,\ 1,\ 0)0s0$ using the notation of Janssen, Janner, Looijenga-Vos & de Wolff (1992), while that for the oxygen subsystem is *Imam* $(x/(2x+1),\ 0,\ 0)00s$, which can be related to the symmetry operators of *Amma* $(1/x,\ 1,\ 0)0s0$ *via* application of the W matrix.

(v) The superspace symmetry operation $\{i\bar{1}|\ 0,\ 0,\ 0,\ 2\delta\}$ fixes the origin in the fourth dimension. With respect to this origin, the M sites (Zr/Nb; site symmetry $mm2$) of the average M substructure occur at $\mathbf{r}_M + \mathbf{T}_M = (1/4)\mathbf{a}_M + 0\mathbf{b}_M + z\mathbf{c}_M + \mathbf{T}_M$ (with $z \simeq 0.21$), while the O sites of the average O substructure occur at $\mathbf{r}_O + \mathbf{T}_O = (1/4 + \delta)\mathbf{a}_O + y\mathbf{b}_O + 1/2\mathbf{c}_O + \mathbf{T}_O$ (with $y \simeq 0.27$). Here $\mathbf{T}_M$ and $\mathbf{T}_O$ are Bravais lattice vectors of the respective parent substructures. Note that the global phase parameter δ fixes the relative positioning along the **a** direction of the M and O substructures at the origin. For the incommensurate refinement δ was zero.

(vi) The symmetry allowed displacive AMF's are given by

$$\begin{aligned}\mathbf{U}_M = \mathbf{a}_M\{&\varepsilon_x(2\mathbf{q}_M)\sin(4\pi[\mathbf{q}_M.(\mathbf{T}_M + \mathbf{r}_M) - \delta]) \\ &+ \varepsilon_x(4\mathbf{q}_M)\sin(8\pi[\mathbf{q}_M.(\mathbf{T}_M + \mathbf{r}_M) - \delta]) + ..\} \\ &+ \mathbf{b}\{\varepsilon_y(\mathbf{q}_M)\sin(2\pi[\mathbf{q}_M.(\mathbf{T}_M + \mathbf{r}_M) - \delta]) \\ &+ \varepsilon_y(3\mathbf{q}_M)\sin(6\pi[\mathbf{q}_M.(\mathbf{T}_M + \mathbf{r}_M) - \delta]) + ..\} \\ &+ \mathbf{c}\{\varepsilon_z(2\mathbf{q}_M)\cos(4\pi[\mathbf{q}_M.(\mathbf{T}_M + \mathbf{r}_M) - \delta]) \\ &+ \varepsilon_z(4\mathbf{q}_M)\cos(8\pi[\mathbf{q}_M.(\mathbf{T}_M + \mathbf{r}_M) - \delta]) + ..\}\end{aligned}$$

and

$$\begin{aligned}\mathbf{U}_O = \mathbf{a}_O\{&\varepsilon_x(2\mathbf{q}_O)\sin(4\pi[\mathbf{q}_O.(\mathbf{T}_O + \mathbf{r}_O)]) \\ &+ \varepsilon_x(4\mathbf{q}_O)\sin(8\pi[\mathbf{q}_O.(\mathbf{T}_O + \mathbf{r}_O)]) + ..\} \\ &+ \mathbf{b}\{\varepsilon_y(2\mathbf{q}_O)\cos(4\pi[\mathbf{q}_O.(\mathbf{T}_O + \mathbf{r}_O)]) \\ &+ \varepsilon_y(4\mathbf{q}_O)\cos(8\pi[\mathbf{q}_O.(\mathbf{T}_O + \mathbf{r}_O)]) + ..\} \\ &+ \mathbf{c}\{\varepsilon_z(\mathbf{q}_O)\sin(2\pi[\mathbf{q}_O.(\mathbf{T}_O + \mathbf{r}_O)]) \\ &+ \varepsilon_z(3\mathbf{q}_O)\sin(6\pi[\mathbf{q}_O.(\mathbf{T}_O + \mathbf{r}_O)]) + ..\},\end{aligned}$$

where the **T**'s are Bravais lattice vectors of the respective M and O substructures. Satellite reflections up to fourth order were taken into account for the refinement (see Tables 2 and 3). The satellite order for any reflection of a composite structure depends upon the particular parent substructure to which it is indexed. Satellite order therefore refers to the minimum possible value with respect to any of the substructures. Fourier terms up to fourth (metal substructure) and eighth order (oxygen substructure) were included in the above displacive AMF's. The final position of the atom μ at the parent substructure position $\mathbf{r}_\mu + \mathbf{T}$ is thus given by $\mathbf{r}_\mu + \mathbf{T} + \mathbf{U}_\mu(\mathbf{r}_\mu + \mathbf{T})$, where $\mathbf{r}_\mu$ is the average position in the asymmetric unit and **T** a Bravais lattice vector of the respective parent substructure.

(vii) Occupational modulation of the metal-atom sites is only allowed for even-order cosine terms as follows

$$\begin{aligned}P_{\mathrm{Zr}}(\mathbf{T}_M + \mathbf{r}_M) = P_{\mathrm{Zr}} &+ P_{\mathrm{Zr}}(2\mathbf{q}_M)\cos(4\pi[\mathbf{q}_M.(\mathbf{T}_M + \mathbf{r}_M) \\ &- \delta]) + P_{\mathrm{Zr}}(4\mathbf{q}_M)\cos(8\pi[\mathbf{q}_M.(\mathbf{T}_M + \mathbf{r}_M) \\ &- \delta])..\end{aligned}$$

with the occupational modulation of Nb fixed by the

relation $P_{Nb} + P_{Zr} = 1$ and average terms set to $P_{Nb} = 1/4$ and $P_{Zr} = 3/4$ (see §2.1).

(viii) The commensurate modulated structure as well as eight-times superstructure refinements were also tried. Given a commensurate primary modulation wavevector and a particular superspace-group symmetry, the corresponding three-dimensional space-group symmetry depends upon the choice made for the global phase parameter δ (see Yamamoto & Nakazawa, 1982; Wiegers, Meetsma, Haange, van Smaalen, de Boer, Meerschaut, Rabu & Rouxel, 1990). For mutually incommensurable substructures all possible relative positionings occur at some point in the crystal and hence the choice of δ can be freely made. However, when $a_O/a_M = 8/17$ exactly, as in the present case, the resulting three-dimensional (supercell) space group is determined by this choice of δ. The allowed three-dimensional space groups can be derived from the above superspace-group symmetry and are given in the present case by $I12/a1$ (for $\delta = 2n/32$, n an integer), $Ima2$ (for $\delta = (2n + 1)/32$) and $I1a1$ (otherwise).

4. Structure refinements

The modulated structure refinements were carried out using the software package *JANA*96 (Petříček, 1996). Scattering factors for neutral atoms were taken from *International Tables for X-ray Crystallography* (1974, Vol. IV). The dispersion corrections $\Delta f'$ and $\Delta f''$ for Zr and Nb were calculated using the computer program *FPRIME* of Cromer & Liberman (1981). Corrections to the relativistic part of the anomalous scattering factors were made following Kissel & Pratt (1990). Unmerged data sets were used for all refinements.†

Initially the refinements were carried out assuming **q** to be incommensurate, *i.e.* assuming all reflections could be uniquely indexed. Starting values for the Fourier coefficients of the displacive terms were taken from the recent structure refinement of the $x = 12$ member (Fütterer *et al.*, 1995). The signs of the dominant Fourier coefficients were systematically varied and the sign combination corresponding to the true minimum was marked by a distinct drop of the residual values. This systematic approach was necessary as it was quite possible to arrive at a false minimum which then prevented the refinement from reaching the true minimum on addition of further refineable parameters. The less dominant parameters were then released, setting the starting values to ± 0.0001. The refinement converged to the same minimum when parameters of increasing harmonic order were released successively. Apart from the parameters of the basic structure, displacive Fourier terms up to fourth order for the metal substructure and up to eighth order for the oxygen substructure were taken into account (see Table 3). Thermal parameter modulation was considered, but found to be unnecessary (see Table 4). The scale factor was refined simultaneously with the other parameters. Refinement was in F with weights as given in Table 2.

Table 4. *Displacement parameters*

Label of Ref.	N2	N5	F2
Zr, Nb			
U^{11}	0.0068 (1)	0.0065 (1)	0.0069 (1)
U^{22}	0.0042 (1)	0.0038 (1)	0.0045 (1)
U^{33}	0.0088 (2)	0.0084 (1)	0.0080 (1)
O			
U^{11}	0.0098 (7)	0.0090 (7)	0.011 (1)
U^{22}	0.0116 (8)	0.0112 (7)	0.012 (1)
U^{33}	0.0112 (9)	0.0111 (8)	0.009 (1)

The intensity data set recorded 8 eV below the Zr K absorption edge (λ_n) was used to investigate the existence of metal ordering in $Nb_2Zr_{x-2}O_{2x+1}$. The average metal site occupancy was set to be 0.75:0.25 (Zr:Nb), as established by compositional analysis using quantitative energy dispersive X-ray spectroscopy (see §2.1). Metal ordering was taken into account by allowing for occupational modulation of the metal site.

Refinement as a commensurately modulated structure was also investigated using an eight-times $\mathbf{a}_M$ superstructure with the value for the global phase, *i.e.* δ, chosen from 0 to 1/8 in steps of 1/32. Symmetry elements were chosen such that the symmetry elements of the superspace group that are not symmetry elements for the resultant three-dimensional space group are still used to constrain parameters in a sensible way. The results of these refinements showed that a choice for the global phase of $\delta = (2n + 1)/32$ gave significantly lower R values than $\delta = 2n/32$. Values of δ between these two

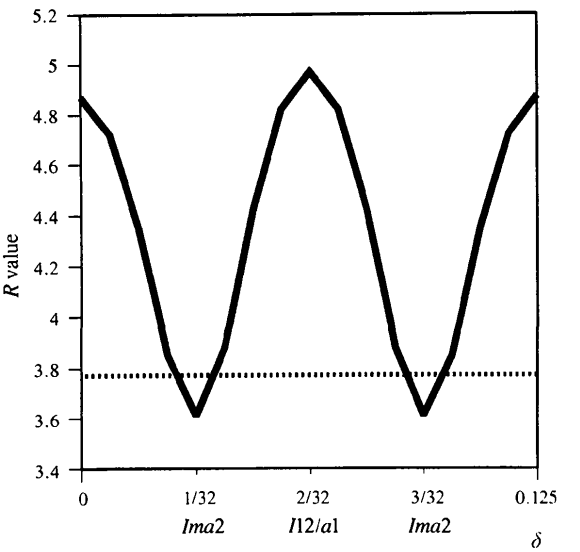

Fig. 1. Plot of R values *versus* δ for refinements as commensurately modulated structures (λ_n; solid line). The dotted line represents the R value for the i.c./overlap (N2) refinement.

†A list of structure factors has been deposited with the IUCr (Reference: BR0063). Copies may be obtained through The Managing Editor, International Union of Crystallography, 5 Abbey Square, Chester CH1 2HU, England.

extremes gave intermediate R values (see Fig. 1). Note, however, that the R values for the incommensurate refinement and for the $\delta = (2n + 1)/32$ commensurately modulated structure refinement were virtually the same (see Fig. 1).

5. Results and discussion

5.1. *General remarks*

Consider a general reflection at $(h + m/8)\mathbf{a}_M^* + (k + m)\mathbf{b}^* + l\mathbf{c}^*$. In four-index notation this reflection can be indexed as $hklm$, but equally validly as $h + 1, k + 8, l, m - 8$ or $h - 1, k - 8, l, m + 8$ *etc.* The unique indexation assumption underpinning the incommensurate structure refinement does not allow more than one such structure-factor contribution to any particular reflection and hence requires a criterion to choose between such alternative possible indexations. For most modulated structures and certainly for $Nb_2Zr_{x-2}O_{2x+1}$ (see Table 3), modulation wave amplitudes diminish sharply with increasing harmonic order so that the strongest contribution to any particular reflection is most likely to arise from the contribution of lowest harmonic order, *i.e.* lowest $|m|$. The criterion used to select an appropriate indexation for the incommensurate structure refinement was therefore to ask which of $|m|$ or $|m - 8|$ was the smaller and to use the corresponding indexation. (Obviously a problem arises for the 22 observed reflections with $m = 4$!.) Applying the W matrix to these indices does not necessarily generate the lowest possible satellite order with respect to the oxygen substructure. The sensitivity of the commensurately modulated structure refinements to the value of the global phase δ (see Fig. 1) demonstrates clearly that overlap occurs and that the unique indexation assumption underpinning the incommensurate structure refinement is not valid, *i.e.* in order to calculate intensities correctly contributions must be included for at least the two lowest-order distinct indexations, *e.g.* for $hklm$ as well as for $h + 1, k + 8, l, m - 8$ [see equation (6) of Pérez-Mato, 1991]. The question then becomes what is the phase relationship between the two lowest-order structure-factor contributions?

In the i.c./overlap refinement (see Table 2) these two lowest-order structure-factor contributions, $A(hklm)$ and $B(h + 1, k + 8, l, m - 8)$ say, are automatically presumed to be orthogonal to each other, so that the calculated intensity is $I = |A|^2 + |B|^2$. In the case of the commensurate modulated structure refinements this relative phase is determined by the choice of global phase δ so that the calculated intensity is $|A|^2 + |B|^2 + 2|A||B|\cos(2\pi.8\delta)$, in the absence of anomalous dispersion. For $\delta = (2n + 1)/32$, I therefore equals $|A|^2 + |B|^2$, explaining the similarity of the refinement statisitics for the i.c./overlap and $\delta = (2n + 1)/32$ commensurate structure refinements. In the case of the incommensurate structure refinement a unique indexation is forced by the above criterion so that I is $|A|^2$. The similarity of the incommensurate structure refinement statistics to those for the i.c./overlap and $\delta = (2n + 1)/32$ commensurate structure refinements suggests that the magnitude of the second structure-factor contribution $B(h + 1, k + 8, l, m - 8)$ must be rather small. Its effect is noticeable, however, particularly in the refinement statistics for the $m = 4$ satellite reflections (see Table 2). These satellite reflections are most likely to be affected by overlap, *i.e.* from $\mathbf{G} + 4\mathbf{q}_M$ and $\mathbf{G}' - 4\mathbf{q}_M$ falling on top of each other.

While there is no apparent conclusion from this discussion as to the best description of the $x = 8$ structure, the linear relationship between $\mathbf{q}$ and x over the compositional range investigated by Thompson *et al.* (1990) together with an equally good fit for the i.c./overlap refinement are clearly in favour of incommensurateness. The following discussion is therefore based on the incommensurate model.

5.2. *Refinement statistics*

Final agreement indices of the refinements labelled N1–N6 (λ_n) and F1–F4 (λ_f) are given in Table 2. Resulting parameters of the three refinements N2, N5 and F2 are given in Tables 3 and 4.

5.3. *The atomic modulation functions*

The refined M and O substructure displacive AMF's are shown in Figs. 2(*a*) and (*b*) as a function of $\mathbf{t}_M = (\mathbf{q}_M.\mathbf{T}_M - \delta)$ and $\mathbf{t}_O = \mathbf{q}_O.(\mathbf{T}_O + \delta\mathbf{a}_O)$, respectively. The metal-atom shifts away from their average positions are quite small – less than 0.15 Å along any basis vector direction. The **a**-axis shifts are almost perfectly sinusoidal, whereas those along the **b** axis are more square-wave-like in appearance. The **c**-axis shifts are virtually negligible. Absolute displacements in the O substructure are much larger – a maximum shift of ~0.75 Å in the **c** direction and displacement amplitudes of ~0.45 Å in both the **a** and **b** directions. The O substructure shifts along any basis vector direction are approximately sinusoidal. The curves for the previously refined member $x = 12$ (Fütterer *et al.*, 1995) are shown as well. Note that some of these curves were wrong in the original paper, due to an unfortunate error in the plot program. The small difference between corresponding curves for the oxygen substructure is due to the differing number of Fourier coefficients that have been included in the refinements.

A comparison of the Fourier coefficients for the present refinement (Table 3) with those of previous refinements (see Table 5, Fütterer *et al.*, 1995) is very instructive. These values reveal a remarkable similarity. The displacement patterns away from the underlying parent substructures not only have the same symmetry, but the series coefficients have the same signs and even their magnitudes are almost the same. It can therefore be concluded that the composite crystal structures of the solid solution members $x = 8$ (present study; Galy &

Roth, 1973) and $x = 12$ (Fütterer *et al.*, 1995) of $Nb_2Zr_{x-2}O_{2x+1}$ are equivalent, not only with respect to their symmetry, but also with respect to their displacive AMF's. Thus, it appears that in these terms all crystal structures occurring in the solid solution are equivalent, except for the magnitude of the wavevector.

5.4. *The coordination sphere*

Fig. 3(*a*) shows a plot of metal–oxygen distances *versus* $\mathbf{t}_M$. Solid lines correspond to the distance variation of a specific metal–oxygen pair with $\mathbf{t}_M$. Due to the model of two interpenetrating and mutually incommensurable substructures, the relative origin of which changes continuously, the distance between a specific metal–oxygen pair goes from infinity to a minimum value and again to infinity for $\mathbf{t}_M$ going from $-\infty$ to $+\infty$. Stacking all relevant metal–oxygen pairs in the coordination sphere of Zr allows one to follow the variation of the metal coordination number with $\mathbf{t}_M$. Distances up to ~2.3 Å result in a coordination number of the metal atom from 6 to 8. Points in the plot, where curve intersections are situated at the same $\mathbf{t}_M$, correspond to special sites in a superstructure description. These points occur at $\mathbf{t}_M$ = 7/32, 15/32, 23/32 and 31/32. Dashed lines represent distances in the average structure. It is readily seen that

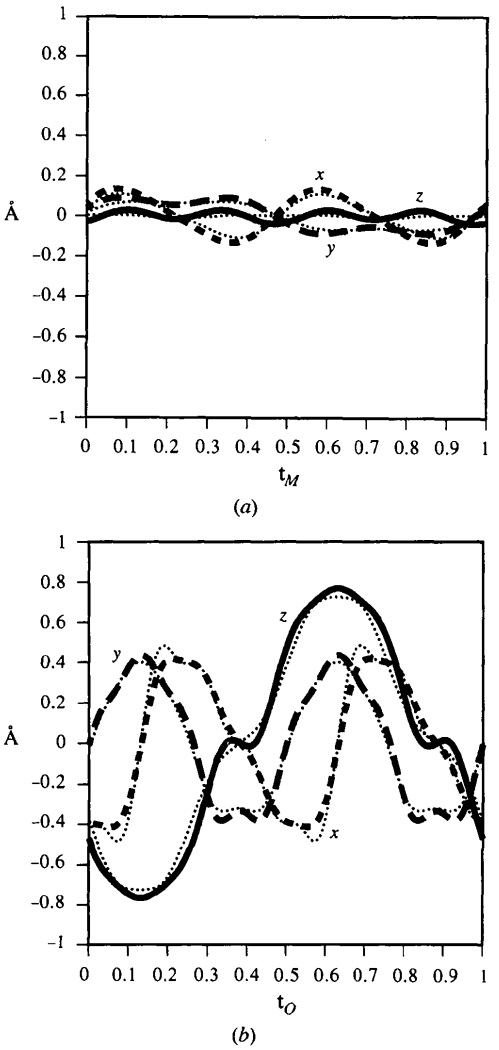

Fig. 2. Final refined metal- and O-atom displacive atomic modulation functions plotted in absolute coordinates as a function of (*a*) $\mathbf{t}_M = (\mathbf{q}_M.\mathbf{T}_M - \delta)$ and (*b*) $\mathbf{t}_O = \mathbf{q}_O.(\mathbf{T}_O + \delta\mathbf{a}_O)$, respectively. Thick lines for $x = 8$, thin dotted lines for $x = 12$.

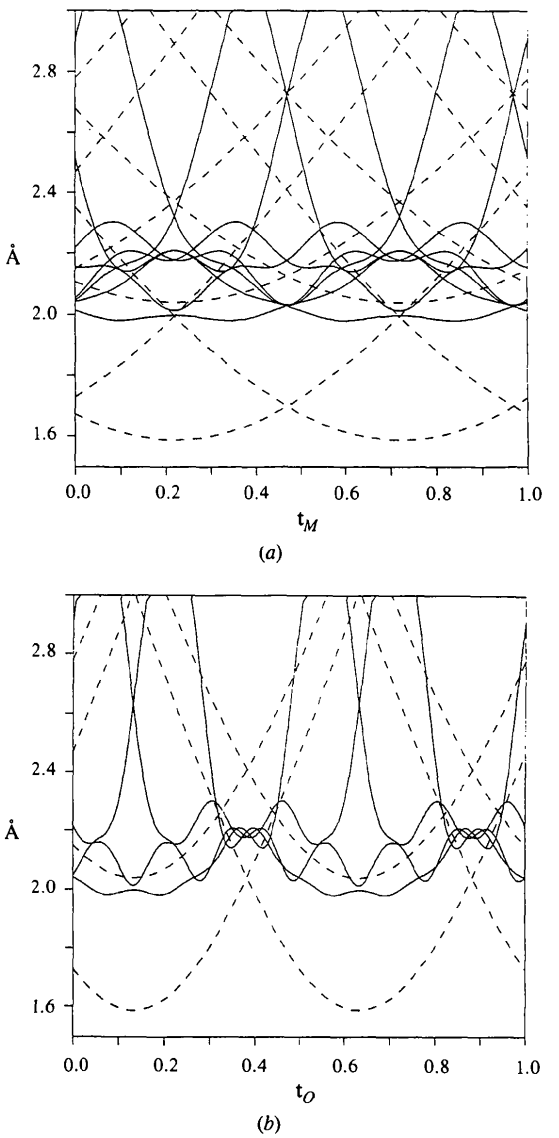

Fig. 3. (*a*) Variation in the metal coordination sphere as a function of $\mathbf{t}_M = (\mathbf{q}_M.\mathbf{T}_M - \delta)$. Each curve represents the distance between a specific metal–oxygen pair (solid lines: modulated structure; dashed lines: average structure). (*b*) Variation in the oxygen coordination sphere as a function of $\mathbf{t}_O = \mathbf{q}_O.(\mathbf{T}_O + \delta\mathbf{a}_O)$. Each curve represents the distance between a specific oxygen–metal pair (solid lines: modulated structure; dashed lines: average structure).

one reason for the modulation is to avoid the minimum distance of 1.6 Å that occurs in the average structure. Fig. 3(*b*) shows the same type of plot for the oxygen as a central atom as a function of $\mathbf{t}_O$.

Fig. 4(*a*) shows part of the structure projected along **c**. The modulation direction is **a**, whereas alternate layers of metal and oxygen substructure are stacked along **b**. The sinusoidal **b**-axis O-atom shifts are clearly visible; the metals hardly move in this projection. The cell outlined corresponds to the repeat of a commensurate modulated structure or an eight-times $\mathbf{a}_M$ superstructure. Fig. 4(*b*) shows the same section in projection along **b** restricting y to $0 \leq y \leq 0.5$ for clarity. The evolution of the oxygen array as a function of the x coordinate is apparent. The oxygen shifts in this projection are rather large and not as smooth as all other displacements.

The non-bonded oxygen–oxygen interaction is assumed to be a limiting factor for the Nb_2O_5-rich end of the solid solution, as the increase of the oxygen:metal ratio would eventually be limited by increasing oxygen–oxygen repulsion. This assumption is apparently supported by the rapidly decreasing **a** lattice parameter of the *O* substructure with decreasing x [$a_O(x = 12) = 2.452$ Å, a_O ($x = 8$) = 2.417 Å]. However, considering the O—O distances for $x = 8$ (see Fig. 5) and $x = 12$ (Fütterer *et al.*, 1995), it turns out that at least the minimum O—O distance is not primarily affected by x, but is found to be essentially the same, *i.e.* ~ 2.5 Å, for both compositions.

5.5. *Metal ordering*

Zr and Nb are neighbouring elements, which renders the detection of metal ordering difficult. Measuring intensity data at $\lambda_f = 0.7495$ Å and $\lambda_n = 0.6892$ Å, $\Delta E = 1450$ and $\Delta E = 8$ eV from the Zr *K* absorption edge, respectively, increases the relative difference of the atomic scattering factors of Zr and Nb from ~ 3 to 16%. This enhanced contrast should then allow the detection of Zr and Nb ordering more easily. The susceptibility of the data sets to composition has been tested by refining the average occupation. The data set measured at λ_f does not allow any sensible refinement, whereas the other data set converges to the correct composition, independent of the starting values. The refinements N2 and N5 differ in that the former assumes a statistical distribution of the metal ions, *i.e.* no substitutional modulation of Zr and Nb, whereas the latter allowed a substitutional modulation. The slightly better residual values of N5 compared with N2 (the differences range from a few tenths of a per cent up to ~ 6% for the fourth-order satellite reflections; see Table 2*a*) seem to suggest the presence of metal ordering. The resulting values of the corresponding Fourier coefficients, describing such substitutional modulation, are $P_{Nb}(2\mathbf{q}) = 0.059\ (7)$ and $P_{Nb}(4\mathbf{q}) = 0.05\ (2)$. However, these values are quite small and it was therefore concluded that if there is a small deviation from random distribution it was not refineable in this way. Difference-Fourier maps show some small features, mainly caused by the higher-order satellites. The maps for both wavelengths, however, look almost the same, suggesting that metal ordering is not present.

Apparent valences (AV's: Brown & Altermatt, 1985; Brese & O'Keeffe, 1991) were calculated for metal and O atoms in the modulated structure using the program *GRAPHT* within the *JANA*96 package (Petříček, 1996). $R_{ij}^0 = 1.931$ was used, reflecting the average metal site occupancy. The resulting AV's gave no indication of metal ordering. The mean AV for the metal sites is $\langle AV_M \rangle = 4.25 \pm 0.15$. For the O atoms one finds $\langle AV_O \rangle = 2.0 \pm 0.04$. The AV's for the metal site are very close to the expected value for a random distribution

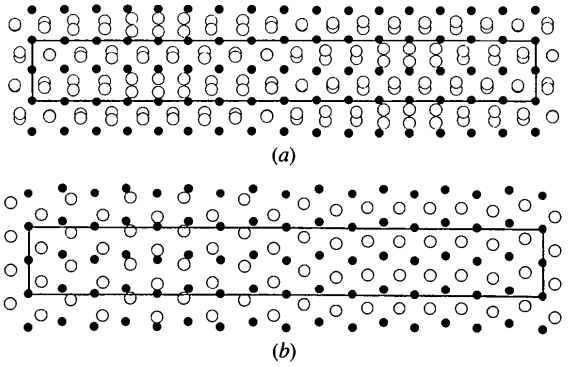

Fig. 4. (*a*) Projection of part of the structure of $Nb_2Zr_{x-2}O_{2x+1}$, $x = 8$, along **c** for $0 \leq z \leq 1$; **b** up the page, **a** to the right. Metal sites are shown as filled circles, oxygen sites are shown as open circles. (*b*) Projection of part of the structure of $Nb_2Zr_{x-2}O_{2x+1}$, $x = 8$, along **b** for $0 \leq y \leq 0.5$ (for clarity); **c** up the page, **a** to the right. Metal sites are shown as filled circles, oxygen sites are shown as open circles.

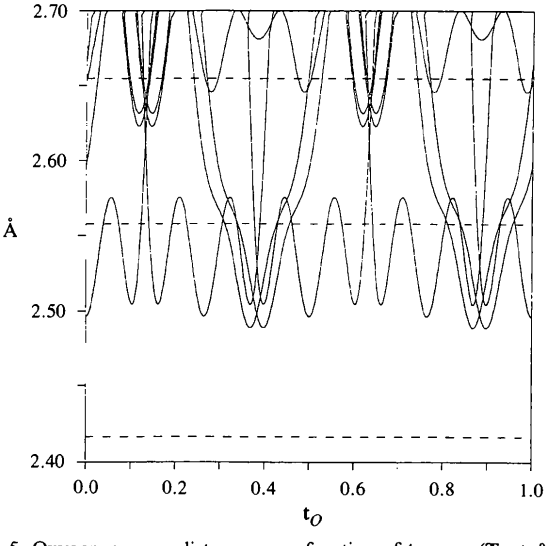

Fig. 5. Oxygen–oxygen distances as a function of $\mathbf{t}_O = \mathbf{q}_O.(\mathbf{T}_O + \delta\mathbf{a}_O)$ (solid lines: modulated structure; dashed lines: average structure).

of metal atoms, *i.e.* 4.25. AV's for $Nb_2Zr_6O_{17}$ were calculated by Fütterer *et al.* (1995) on the basis of coordinates reported by Galy & Roth (1973). A larger scattering of AV's around the mean value was observed, *i.e.* $\langle AV_M \rangle = 4.416 \pm 0.254$ and $\Delta_{max} = 0.332$, $\langle AV_O \rangle = 2.076 \pm 0.061$, $\Delta_{max} = 0.108$. However, AV's based on the Fourier decomposition of Withers *et al.* (1991), omitting terms of higher order than fourth, substantially reduced the range of AV's whilst the average value remained the same within a standard deviation, *i.e.* $\langle AV_M \rangle = 4.401 \pm 0.013$.

Therefore, calculation of AV's as well as the refinement results themselves strongly suggest that there is no long-range metal ordering.

6. Conclusion

Composite modulated structure refinements at opposite ends of the wide-range non-stoichimetric $Nb_2Zr_{x-2}O_{2x+1}$ ($7.1 \leq x < 12$) solid-solution field have been shown to have essentially the same Fourier amplitudes and phases, despite the large change in composition. Long-range metal ordering has been shown to be negligible and seems to be of minor importance for the understanding of the crystal structure.

The authors acknowledge helpful discussions with Professor A. D. Rae. A major part of the experimental work has been made possible by funding from the Access to Major Research Facilities fund of the Australian Federal Government and the generous allocation of beamtime by the Photon Factory, National Laboratory for High Energy Physics, Tsukuba, Japan (Project no. 94G136). Furthermore, a grant from the Grant Agency of the Czech Republic (no. 202/96/0085), invaluable for the development of *JANA*96, is gratefully acknowledged.

References

Brese, N. E. & O'Keeffe, M. (1991). *Acta Cryst.* B**47**, 192–197.
Brown, I. D. & Altermatt, D. (1985). *Acta Cryst.* B**41**, 244–247.
Cromer, D. T. & Liberman, D. A. (1981). *Acta Cryst.* A**37**, 267–268.
Fütterer, K., Schmid, S., Thompson, J. G., Withers, R. L., Ishizawa, N. & Kishimoto, S. (1995). *Acta Cryst.* B**51**, 688–697.
Galy, J. & Roth, R. S. (1973). *J. Solid State Chem.* **7**, 277–285.
Hall, S. R., Flack, H. D. & Stewart J. M. (1992). Editors. *Xtal*3.2. *Reference Manual*. Universities of Western Australia, Australia, Geneva, Switzerland, and Maryland, USA.
Janssen, T., Janner, A., Looijenga-Vos, A. & de Wolff, P. M. (1992). *International Tables for Crystallography*, edited by A. J. Wilson, Vol. C, pp. 797–835. Dordrecht: Kluwer Academic Publishers.
Kissel, L. & Pratt, R. H. (1990). *Acta Cryst.* A**46**, 170–175.
Makovicky, E. & Hyde, B. G. (1981). *Struct. Bonding*, **46**, 101–170.
Makovicky, E. & Hyde, B.G. (1992). *Mater. Sci. Forum*, **100–101**, 1–100.
Pérez-Mato, J. M. (1991). In *Methods of Structural Analysis of Modulated Structures and Quasi-Crystals*, edited by J. M. Pérez-Mato, F. J. Zúñiga & G. Madariaga, pp. 117–128. Singapore: World Scientific.
Pérez-Mato, J. M., Madariaga, G., Zúñiga, F. J. & Garcia Arribas, A. (1987). *Acta Cryst.* A**43**, 216–226.
Petříček, V. (1996). *JANA*96. *Programs for Modulated and Composite Crystals*. Institute of Physics, Praha, Czech Republic.
Rinck, C. (1982). Ph.D. Thesis. Universität Karlsruhe, Germany.
Roth, R. S. (1981). *Prog. Solid State Chem.* **13**, 159–192.
Roth, R. S., Waring, J. L., Brower, W. S. & Parker, H. S. (1972). Solid State Chemistry, Proceedings of the 5th Materials Research Symposium, pp. 183–195. National Bureau of Standards Special Publication 364.
Satow, Y. & Iitaka, Y. (1989). *Rev. Sci. Instrum.* **60**, 2390–2393.
Schmid, S., Thompson, J. G., Rae, A. D., Butler, B. D., Withers, R. L., Ishizawa, N. & Kishimoto, S. (1995). *Acta Cryst.* B**51**, 698–708.
Schmid, S. & Withers, R. L. (1994). *J. Solid State Chem.* **109**, 391–400.
Schmid, S. & Withers, R. L. (1996). *Aust. J. Chem.* **49**, 827–833.
Schmid, S., Withers, R. L. & Thompson, J. G. (1992). *J. Solid State Chem.* **99**, 226–242.
Smaalen, S., van (1991). *Phys. Rev. B*, **43**, 11330–11341.
Smaalen, S., van (1995). *Cryst Rev.* **4**, 79–202.
Thompson, J. G., Withers, R. L., Sellar, J., Barlow, P. J. & Hyde, B. G. (1990). *J. Solid State Chem.* **88**, 465–475.
Wiegers, G. A., Meetsma, A., Haange, R. J., van Smaalen, S., de Boer, J. L., Meerschaut, A., Rabu, P. & Rouxel, J. (1990). *Acta Cryst.* B**46**, 324–332.
Withers, R. L., Thompson, J. G. & Hyde, B. G. (1991). *Acta Cryst.* B**47**, 166–174.
Yamamoto, A. & Nakazawa, H. (1982). *Acta Cryst.* A**38**, 79–86.